Anisotropy and morphology of strained III-V heteroepitaxial films

Lawrence H. Friedman
Department of Engineering Science and Mechanics, Penn State University, 212 Earth and Engineering Sciences Building, University Park, Pennsylvania 16802, USA

(Received 15 April 2008; revised manuscript received 21 August 2008; published 6 November 2008)

Strained coherent heteroepitaxy of III-V semiconductor films such as $In_xGa_{1-x}As/GaAs$ has potential for electronic and optoelectronic applications such as high density logic, quantum computing architectures, laser diodes, and other optoelectronic devices. Crystal symmetry can have a large effect on the morphology of these films and their spatial order. Often the formation of group IV strained heterostructures such as Ge deposited on Si is analyzed using analytic models based on the Asaro-Tiller-Grinfeld instability. However, the governing dynamics of III-V three-dimensional heterostructure formation has different symmetry and is more anisotropic. The additional anisotropy appears in both the surface energy and diffusivity. Here, the resulting anisotropic governing dynamics are studied to linear order. The resulting possible film morphologies are compared with experimentally observed $In_xGa_{1-x}As/GaAs$ films. Notably it is found that surface-energy anisotropy plays a role at least as important as surface-diffusion anisotropy if not more so, in contrast to previous suppositions.

DOI: 10.1103/PhysRevB.78.193302 PACS number(s): 81.16.Rf, 81.07.Ta, 81.15.Aa, 81.16.Dn

Strained coherent heteroepitaxy of $In_xGa_{1-x}As/GaAs$ at high temperatures can lead to dense somewhat correlated three-dimensional (3D) film growth, for example, rolls [Figs. 2(c) and 2(d) in Ref. 1], as well as correlated dense arrays of self-assembled quantum dots (SAQDs) (Fig. 1 in Ref. 2) and quantum dot chains in multilayers [Fig. 1(a) in Ref. 3]. These structures are of great interest for the next generation of electronic and optoelectronic materials due to their quantum confinement effects,[4] and they are an excellent example of nanoscale self-assembly that can augment or replace traditional lithographic techniques. The density and degree of correlation in these film morphologies suggest that their growth is barrierless and cooperative. Furthermore, these structures form at high temperature, suggesting that the surfaces might be thermally roughened. Thus, the film morphology is likely governed by the Asaro-Tiller-Grinfeld (ATG) instability or related mechanism, whereby surface diffusion is driven by changes in elastic and surface energy.[5–9] Unlike modeling group IV structures (e.g., Ge_xSi_{1-x}/Si),[10,11] modeling the growth of III-V heterostructures as an ATG-type process requires full consideration of three contributions to anisotropic pattern formation, namely, elastic anisotropy, surface-energy density anisotropy, and diffusion anisotropy. The role of anisotropic effects has been increasingly recognized in nanoscale epitaxial self-assembly.[12–14] Here, a linear model is presented that has appropriate symmetries for III-V structures generally, and $In_xGa_{1-x}As/GaAs$ in particular.

Similar models have been largely applied to group IV heteroepitaxy, such as Ge_xSi_{1-x}/Si, that have fourfold rotational symmetry of the crystal surface, but III-V systems have only twofold rotational symmetry. The experimental observations bear out this difference. $In_xGa_{1-x}As/GaAs$ structures grown on (001) surfaces form rows or rolls that are aligned closer to the $[1\bar{1}0]$ direction than the [110] direction. On the other hand, Ge_xSi_{1-x}/Si structures form a fourfold-symmetric pattern with alignment along the $\langle 100\rangle$ directions.[15] This spatial alignment of $In_xGa_{1-x}As/GaAs$ structures closer to the $[1\bar{1}0]$ direction has been attributed to differences in surface diffusivity[1–3] and possibly to packing effects and surface faceting.[1] To test these hypotheses, one must obtain similar structures from a complete model of surface evolution. A linear analysis of surface diffusion based on the original ATG instability has been used to explain anisotropic patterning in Ge_xSi_{1-x}/Si heteroepitaxy,[10,11] and it would be remiss not to apply it to $In_xGa_{1-x}As/GaAs$. In group IV systems, the symmetry requirements forbid anisotropic surface-energy and diffusion effects to linear order.[16] Thus, for Ge_xSi_{1-x}/Si the $\langle 100\rangle$ alignment comes from elastic anisotropy. The lower symmetry of III-V (001) surfaces allows surface-energy and diffusion anisotropy effects; thus, all three contributions interact to determine the alignments of 3D morphological features.

In the following, a continuum linear model of anisotropic film evolution is presented including the general framework, then energetic and diffusional sources of anisotropy. Then the consequences for film morphology are presented and compared with experimental observations.

Early stage small fluctuations in film height are an important determiner for final film morphology[7–9] and can be analyzed using linear dynamics of the film height that is a sum of the average film height ($\bar{\mathcal{H}}$) and film height fluctuations [$h(\mathbf{x},t)$], $\mathcal{H}(\mathbf{x},t)=\bar{\mathcal{H}}+h(\mathbf{x},t)$. The normal modes of the film evolution are periodic; thus, Fourier components of the height fluctuations are used; $h_{\mathbf{k}}=A^{-1}\int d^2\mathbf{x}e^{-i\mathbf{k}\cdot\mathbf{x}}h(\mathbf{x})$ and $h(\mathbf{x})=\Sigma_{\mathbf{k}}e^{i\mathbf{k}\cdot\mathbf{x}}h_{\mathbf{k}}$, where A is the area of the substrate, and periodic boundary conditions are assumed. Following Ref. 17, each Fourier component is initially governed by energy dissipation and thermal fluctuations,

$$\partial_t h_{\mathbf{k}} = \sigma(\mathbf{k})h_{\mathbf{k}} + i\mathbf{k}\cdot\sqrt{2k_bT\mathbf{D}}\cdot\eta_{\mathbf{k}},$$

$$\sigma(\mathbf{k}) = -(\mathbf{k}\cdot\mathbf{D}\cdot\mathbf{k})f(\mathbf{k}), \qquad (1)$$

where $\sigma(\mathbf{k})$ is the dispersion relation, $\mathbf{D}$ is the surface diffusivity, $\eta_{\mathbf{k}}(t)$ is a normally distributed stochastic variable with mean $\langle\eta_{\mathbf{k}}(t)\rangle=0$, and variance $\langle\eta_{\mathbf{k}}(t)\eta^*_{\mathbf{k}'}(t')\rangle=A^{-1}\delta_{\mathbf{k}\mathbf{k}'}\delta(t-t')$. $\delta_{\mathbf{k}\mathbf{k}'}$ is the Kronecker delta, $\delta(t-t')$ is the Dirac delta, and $f(\mathbf{k})$ is the energy cost function, formally

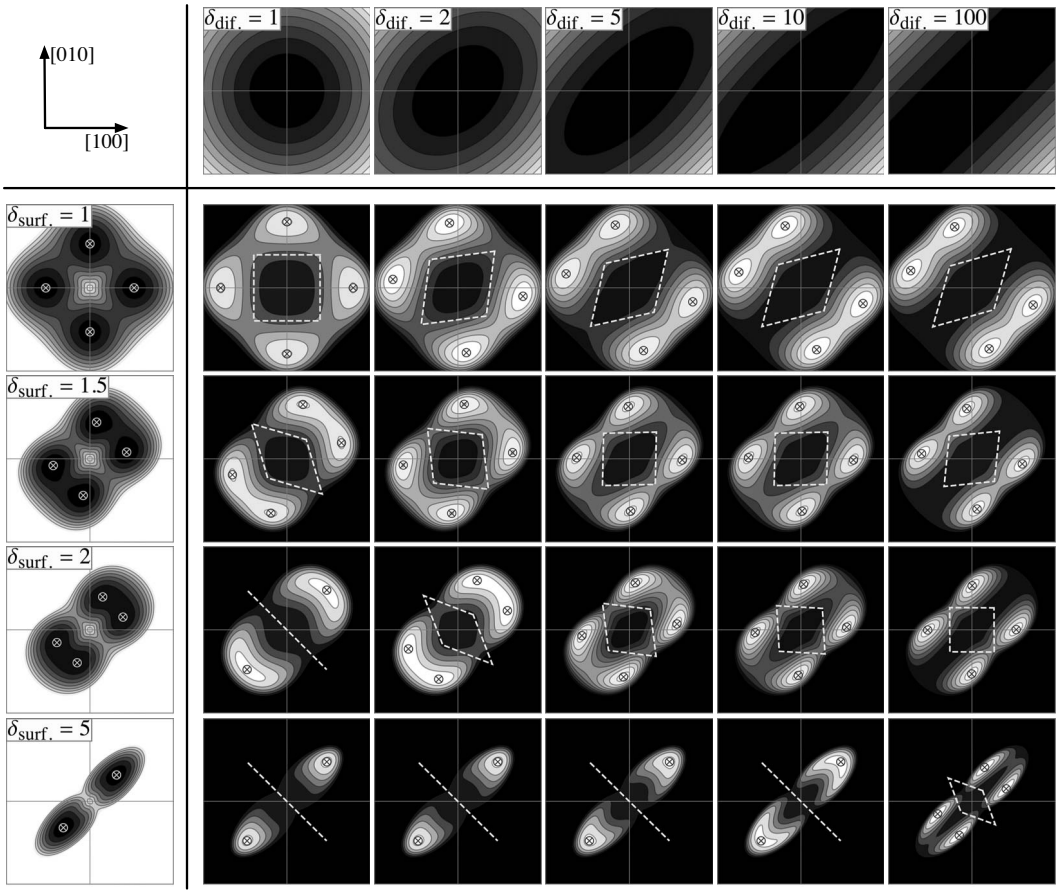

FIG. 1. *Graphical "multiplication table"* showing effects of diffusional and surface-energy anisotropy. Top row shows $(\mathbf{k}\cdot\mathbf{D}\cdot\mathbf{k})/D_0$ for various surface-diffusion anisotropies $\delta_{\text{dif.}}$. Left column shows $f(\mathbf{k})$ for various surface-stiffness anisotropies $\delta_{\text{surf.}}$. Interior grid shows resulting dispersion relation $\sigma(\mathbf{k})$ [Eq. (1)]. Horizontal direction (→) is [100]. Vertical direction (↑) is [010]. All axes span ±1 rad/nm. ⊗'s indicate $\mathbf{k}_E$ for $f(\mathbf{k})$ and $\mathbf{k}_0$ for $\sigma(\mathbf{k})$ plots. Dashed lines perpendicular to $\mathbf{k}_0$ indicate mean alignment of grating rows or rolls (Fig. 2).

defined as the second derivative of the free energy per unit area $(\mathcal{F}/A)$ with respect to each Fourier component,

$$f(\mathbf{k}) = \partial_{h_\mathbf{k}} \partial_{h_\mathbf{k}^*} (\mathcal{F}/A)|_{h_\mathbf{k}=0}. \tag{2}$$

From $\sigma(\mathbf{k})$, one can determine various length and time scales, as well as pattern orientation and alignment.

The film free-energy cost function consists of two terms due to elastic strain and surface energy, $f(\mathbf{k}) = f_{\text{elast.}}(\mathbf{k}) + f_{\text{surf.}}(\mathbf{k})$. For now, the wetting energy contribution[18] is neglected for simplicity. For a (001) surface, elastic anisotropy leads to fourfold-symmetric surface energetics and dynamics, and surface-energy anisotropy leads to twofold symmetric energetics and dynamics as explained below.

The effect of elastic anisotropy alone has been discussed previously,[10,11,16,19] and the most important results are summarized below. For (001) surfaces, the elastic part of the energy cost function can be approximated as[16]

$$f_{\text{elast.}}(\mathbf{k}) = -[\mathcal{E}_{0^\circ} \cos^2(2\theta_\mathbf{k}) + \mathcal{E}_{45^\circ} \sin^2(2\theta_\mathbf{k})]k, \tag{3}$$

where $\mathcal{E}_{0^\circ}$ and $\mathcal{E}_{45^\circ}$ are constants, $\theta_\mathbf{k}$ is the angle between $\mathbf{k}$ and the [100] direction, and $k = \|\mathbf{k}\|$. $f_{\text{elast.}}$ is most negative along the ⟨100⟩ directions; thus, ripples perpendicular to these directions release the most elastic energy. Without competing anisotropic effects, the anisotropy of $f_{\text{elast.}}$ causes initial alignment of 3D gratings along the ⟨100⟩ directions.[10,11] For InAs, $\mathcal{E}_{0^\circ} = 8.13 \times 10^9$ erg/cm^3 and $\mathcal{E}_{45^\circ} = 6.92 \times 10^9$ erg/cm^3.

One can derive the general form of $f_{\text{surf.}}$ as follows. Assume that the total free energy is an integral in the $\mathbf{x}$-plane over a local free-energy kernel ω that depends on the surface orientation $\nabla\mathcal{H}$, $\mathcal{F}_{\text{surf.}} = \int d^2\mathbf{x}\omega[\nabla\mathcal{H}(\mathbf{x})]$. In terms of the surface-energy density γ, $\omega = \gamma(\nabla\mathcal{H})\{1 + [\nabla\mathcal{H}(\mathbf{x})]^2\}^{1/2}$. Using Eq. (2), the free-energy cost function is

$$f_{\text{surf.}}(\mathbf{k}) = \mathbf{k} \cdot \tilde{\omega}'' \cdot \mathbf{k}, \tag{4}$$

where $\tilde{\omega}'' = \partial^2_{\nabla\mathcal{H}} \omega|_{\nabla\mathcal{H}=\mathbf{0}} = \gamma(\mathbf{0})\tilde{\mathbf{I}} + \tilde{\gamma}'(\mathbf{0})$. $\tilde{\omega}''$ acts like a surface stiffness stabilizing short wavelengths.[16]

From Eq. (4), one can determine the possible form of any anisotropy. $\tilde{\omega}''$ is a rank 2, dimension 2, symmetric tensor, and it has two eigenvalues and eigenvectors. Due to crystal symmetry, namely, reflections through the (110) and $(1\bar{1}0)$ planes, the eigenvectors of $\tilde{\omega}''$ must be in the [110] and $[1\bar{1}0]$ directions with eigenvalues $\omega_{[110]}$ and $\omega_{[1\bar{1}0]}$. The surface-energy anisotropy coefficient can be defined as $\delta_{\text{surf.}} = \omega_{[1\bar{1}0]}/\omega_{[110]}$ so that $\tilde{\omega}'' = \omega_0(\mathbf{n}_{[110]}\mathbf{n}_{[110]} + \delta_{\text{surf.}}\mathbf{n}_{[1\bar{1}0]}\mathbf{n}_{[1\bar{1}0]})$, where $\omega_0 = \omega_{[110]}$, $\mathbf{n}_{[\ldots]}$ is the unit vector in the specified di-

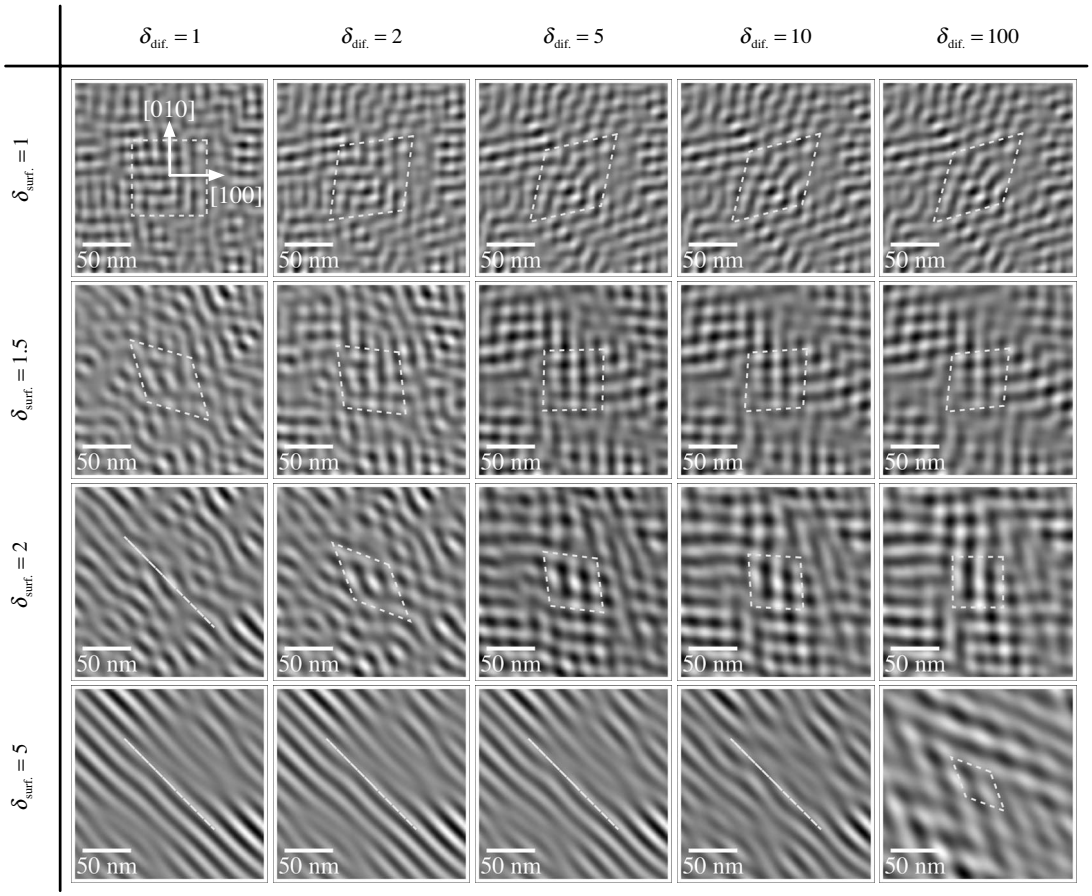

FIG. 2. "Simulated" film heights for various values of $\delta_{\text{dif.}}$ and $\delta_{\text{surf.}}$ corresponding to $\sigma(\mathbf{k})$'s appearing in Fig. 1. All figures oriented with [100] horizontal (→) and [010] vertical (↑). Dashed lines show mean grating or roll alignment predicted by $\sigma(\mathbf{k})$.

rection, and the vector products are outer products. Thus, $\delta_{\text{surf.}}=1$ indicates an isotropic surface stiffness, and $\delta_{\text{surf.}}>1(<1)$ indicates an enhanced stiffness in the $\pm[1\bar{1}0](\pm[110])$ directions. In terms of the surface-energy density, $\delta_{\text{surf.}}=(\gamma(\mathbf{0})+\gamma_{[1\bar{1}0]})/(\gamma(\mathbf{0})+\gamma_{[110]})$, where $\gamma_{[\ldots]}$ are the eigenvalues of $\tilde{\gamma}''$.

The exact values of ω_0 and $\delta_{\text{surf.}}$ are not known, so ω_0 will be taken to be about 770 erg/cm^2.[20] Then, taking in turn $\delta_{\text{surf.}}=1$, 1.5, 2, and 5 the total energy cost functions are shown on the left-hand column of Fig. 1. Only values of $\delta_{\text{surf.}}\geq 1$ are shown, corresponding to enhanced stiffness in the $\pm[1\bar{1}0]$ directions.

In all cases, the energy cost function has negative minima indicating the wave vectors of the energetically most unstable modes, $\mathbf{k}_E$. In agreement with previous findings,[10,11] for the isotropic surface-energy case, $\mathbf{k}_E$ point along the $\langle 100\rangle$ directions with magnitude $k_E=\mathcal{E}_{0^\circ}/(2\omega_0)$. However, for $\delta_{\text{surf.}}>1$, the peak wave vectors move toward the $\pm[110]$ directions, and the magnitudes decrease so that $k_E<\mathcal{E}_{0^\circ}/(2\omega_0)$. For $\delta_{\text{surf.}}>2.4$, the peaks actually merge to form one peak with $\mathbf{k}_E$ along the $\pm[110]$. An opposite trend would be found for $\delta_{\text{surf.}}<1$ (not shown).

In addition to energetics, one must consider dynamics. The surface diffusivity is a rank 2, dimension 2, tensor, and it must have the same symmetry as the crystal surface. Thus, it has two eigenvectors and eigenvalues corresponding to the $[110]$ and $[1\bar{1}0]$ directions just as $\tilde{\omega}''$ does. Let $\delta_{\text{dif.}}=D_{[110]}/D_{[1\bar{1}0]}$ and $D_0=D_{[110]}$. Then, $\tilde{\mathbf{D}}=D_0(\delta_{\text{dif.}}^{-1}\mathbf{n}_{[110]}\mathbf{n}_{[110]}+\mathbf{n}_{[1\bar{1}0]}\mathbf{n}_{[1\bar{1}0]})$. $\delta_{\text{dif.}}>1$ indicates slower diffusion in the $[110]$ direction, which is believed for As-terminated $(001)B$ InAs.[21] The top row of Fig. 1 shows $(\mathbf{k}\cdot\tilde{\mathbf{D}}\cdot\mathbf{k})/D_0$ for $\delta_{\text{dif.}}=1$, 2, 5, 10, and 100.

Three contributions to anisotropy in surface morphology have been discussed. The first two, elastic anisotropy and surface-stiffness anisotropy, contribute to an anisotropic energy cost function, $f(\mathbf{k})$. The last, diffusional anisotropy, multiplies $f(\mathbf{k})$ to give an anisotropic dispersion relation $\sigma(\mathbf{k})$ [Eq. (1)]. The peaks in $\sigma(\mathbf{k})$ give the fastest growing perturbation wave vectors, $\mathbf{k}_0$. Figure 1 shows a figurative multiplication table of the combined effects of surface-stiffness anisotropy and diffusive anisotropy on the dispersion relation. The left column and top row show the surface-stiffness and diffusivity anisotropy, respectively, while the inner grid shows the combined effects. Resulting real-space morphological alignments for each case will be perpendicular to $\mathbf{k}_0$ and are shown by dashed lines in Fig. 1.

From examination of Fig. 1 and calculations using other $\delta_{\text{surf.}}$ and $\delta_{\text{dif.}}$ values (not shown), one finds:

(1) When only elasticity is anisotropic ($\delta_{\text{surf.}}=\delta_{\text{dif.}}=1$), the peaks are oriented along the $\langle 100\rangle$ directions, the same as the peaks in $f(\mathbf{k})$, but the magnitudes $k_0=|\mathbf{k}_0|=(3/2)k_E=3\omega_0/(4\mathcal{E}_{0^\circ})$ as expected.[9,16]

(2) When $\delta_{\text{dif.}}>1$ and $\delta_{\text{surf.}}=1$, diffusivity is greater in the "fast" $[1\bar{1}0]$ direction, but with isotropic surface stiffness the peaks move toward the fast $\pm[1\bar{1}0]$ directions, and the magnitude k_0 decreases.

(3) When $\delta_{\text{dif.}}=1$, but $\delta_{\text{surf.}}>1$, the peaks move toward the "slow" $\pm[110]$ directions. In particular, for $\delta_{\text{surf.}}>1.94$, the pairs of peaks in the $\pm[110]$ directions each merge into one peak exactly along the $\pm[110]$ directions. Note that the energetic minima at $\mathbf{k}_E$ merge at values, $\delta_{\text{surf.}}>2.4$.

(4) When $\delta_{\text{dif.}}>1$, and $\delta_{\text{surf.}}>1$, the two effects compete. For example, for $\delta_{\text{dif.}}=100$ and $\delta_{\text{surf.}}=2$, the peak positions $\mathbf{k}_0$ appear almost exactly along the $\langle 100\rangle$ axes, and for large $\delta_{\text{surf.}}$ and $\delta_{\text{dif.}}$, for example, $\delta_{\text{surf.}}=5$ and $\delta_{\text{dif.}}=100$, the merged peaks in $f(\mathbf{k})$ are split by the anisotropic surface diffusivity back into four peaks that appear near the slow $\pm[110]$ directions.

The initial film morphology will be quasiperiodic with reciprocal lattice vectors given by the peaks in $\sigma(\mathbf{k})$ (Fig. 1). For visualization, one can sample film height fluctuations from the appropriate statistical distribution. Following Ref. 17, Eq. (1) is used to find the ensemble means and variances of the individual film height Fourier components. Taking the ensemble average of Eq. (1), $\partial_t\langle h_{\mathbf{k}}\rangle=\sigma(\mathbf{k})\langle h_{\mathbf{k}}\rangle$. Since initially $\langle h_{\mathbf{k}}\rangle=0$, $\langle h_{\mathbf{k}}\rangle=0$ for all t. Using the stochastic chain rule for $\partial_t|h_k|^2$ and taking an ensemble average, $\partial_t\langle|h_k|^2\rangle=2\sigma_{\mathbf{k}}\langle|h_k|^2\rangle+2k_bT(\mathbf{k}\cdot\mathbf{D}\cdot\mathbf{k})/A$. Solving, $\langle|h_{\mathbf{k}}|^2\rangle=k_bT(e^{2\sigma(\mathbf{k})t_{\text{large}}}-1)/[Af(\mathbf{k})]$, where t_{large} is chosen so that the rms film height fluctuation is an appropriate value for small fluctuations, $h_{\text{r.m.s}}=(\Sigma_{\mathbf{k}}\langle|h_{\mathbf{k}}|^2\rangle)^{1/2}=2.5$ Å.

Figure 2 shows sampled initial film morphologies corresponding to the dispersion relations $\sigma(\mathbf{k})$ from Fig. 1. Dashed lines in both figures are perpendicular to $\mathbf{k}_0$ and show the mean orientations of either grating rows or rolls. Dispersion relations $[\sigma(\mathbf{k})]$ with four peaks lead to quasiperiodic gratings that are suitable precursors to self-assembled quantum dots. Dispersion relations with two peaks lead to roll structures. These structures, however, might evolve significantly during later development perhaps in a fashion similar to ripening. Such evolution might depend in detail on the surface-energy density $\gamma(\nabla\mathcal{H})$ to higher than linear order and is thus a subject for future investigation.

Figures 1 and 2 indicate that fast diffusion in the $[1\bar{1}0]$ direction alone cannot be responsible for the observation of film morphologies aligned either along or close to the $[1\bar{1}0]$ direction.[1–3] In fact, it gives the opposite result, alignment close to the slow [110] direction. $[1\bar{1}0]$-aligned patterns occur either for moderate values of $\delta_{\text{surf.}}$ and small or zero $\delta_{\text{dif.}}$, or for the case where both $\delta_{\text{surf.}}$ and $\delta_{\text{dif.}}$ are large. It is generally accepted that the $[1\bar{1}0]$ direction is the fast diffusion direction,[21] suggesting that the latter case is more likely than the former. As mentioned above, $\delta_{\text{surf.}}<1$ would have the opposite effect; thus, observations of SAQD arrangements can be used to infer that $\delta_{\text{surf.}}>1$. A Fourier transform of Fig. 1 from Ref. 2 has broad peaks that overlap the slow [110] directions significantly. Perhaps the spectral support along the [110] direction is initially suppressed by diffusional anisotropy and appears later due to nonlinear effects, which will be the subject of future investigations. The other mentioned images from Refs. 1 and 3 have spectral support that is close to the [110] direction but with less overlap.

A linear surface-evolution model was presented that incorporates elastic, surface-energy, and diffusional anisotropy. It was found that fast diffusion in the $[1\bar{1}0]$ direction gives initial morphology aligned along the slow [110] direction. Thus, observed $[1\bar{1}0]$-directed alignment of morphology[1–3] must be caused in whole or in part by surface-energy anisotropy. Future nonlinear modeling is needed to confirm this observation and may reveal even more complicated mechanisms.

Thanks to G. Salamo and Zh. Wang (University of Arkansas) and J. Millunchick (University of Michigan) for useful discussions.

[1] N. S. Chokshi and J. M. Millunchick, Appl. Phys. Lett. **76**, 2382 (2000).
[2] B. L. Liang, Z. M. Wang, Y. I. Mazur, V. V. Strelchuck, K. Holmes, J. H. Lee, and G. J. Salamo, Nanotechnology **17**, 2736 (2006).
[3] M. Schmidbauer, S. Seydmohamadi, D. Grigoriev, Z. M. Wang, Y. I. Mazur, P. Schafer, M. Hanke, R. Kohler, and G. J. Salamo, Phys. Rev. Lett. **96**, 066108 (2006).
[4] D. Bimberg, M. Grundmann, and N. N. Ledentsov, *Quantum Dot Heterostructures* (Wiley, New York, 1999).
[5] R. Asaro and W. Tiller, Metall. Trans. B **3**, 1789 (1972).
[6] M. Y. Grinfeld, Sov. Phys. Dokl. **31**, 831 (1986).
[7] D. J. Srolovitz, Acta Metall. **37**, 621 (1989).
[8] B. J. Spencer, P. W. Voorhees, and S. H. Davis, J. Appl. Phys. **73**, 4955 (1993).
[9] A. A. Golovin, S. H. Davis, and P. W. Voorhees, Phys. Rev. E **68**, 056203 (2003).
[10] C. S. Ozkan, W. D. Nix, and H. J. Gao, J. Mater. Res. **14**, 3247 (1999).
[11] Y. Obayashi and K. Shintani, J. Appl. Phys. **84**, 3141 (1998).
[12] A. Pradhan, N.-Y. Ma, and F. Liu, Phys. Rev. B **70**, 193405 (2004).
[13] H. J. W. Zandvliet and R. van Gastel, Phys. Rev. Lett. **99**, 136103 (2007).
[14] G. E. Thayer, J. B. Hannon, and R. M. Tromp, Nature Mater. **3**, 95 (2004).
[15] C. S. Ozkan, W. D. Nix, and H. Gao, Appl. Phys. Lett. **70**, 2247 (1997).
[16] L. H. Friedman, J. Nanophotonics **1**, 013513 (2007).
[17] L. H. Friedman, J. Electron. Mater. **36**, 1546 (2007).
[18] M. J. Beck, A. van de Walle, and M. Asta, Phys. Rev. B **70**, 205337 (2004).
[19] L. H. Friedman, Phys. Rev. B **75**, 193302 (2007).
[20] E. Pehlke, N. Moll, and M. Scheffler, arXiv:cond-mat/9612004 (unpublished).
[21] K. Shiraishi, Appl. Phys. Lett. **60**, 1363 (1992).